LED Current Balancing Scheme Using Current-Fed Quasi-Z-Source Converter

Daheon Hong and Honnyong Cha, *Senior Member, IEEE*

***Abstract*—This article presents a novel two-channel light emitting diode (LED) current balancing method using current-fed (CF) quasi-Z-source (qZS) dc–dc converter. The proposed LED driver is simple in structure and requires minimal number of component counts. Currents flowing through the two LED strings are automatically balanced owing to charge (amp–sec) balance condition on capacitors in the CF–qZS network. Since current balancing is achieved automatically by passive components, current control of the proposed converter is very simple. In addition, the proposed circuit uses only one active switch and one diode. The operating principle and characteristics of the proposed two-channel LED driver are analyzed in detail. To verify validity of the proposed converter, 80 W prototype is built and tested.**

***Index Terms*—Charge balance condition, current balancing, current-fed (CF), LED current balancing, quasi-z-source (qZS) network.**

I. Introduction

LIGHT emitting diodes (LEDs) are widely used in residential, automotive, and medical applications owing to its advantages such as long lifetime, small size, high illumination efficiency, and environmentally friendly characteristics [1]. In general, LEDs are connected in multistring (or -channel) structure to avoid high voltage of a series connected structure and to ensure sufficient output illumination intensity [2]. However, current balancing is crucial in multistring structure because the brightness of LED is directly related to its forward current [3].

There are several methods to balance string currents in multistring LED drivers. Fig. 1(a) shows an active method of LED current balancing where individual current controller is used to control each LED current evenly. This method, however, is complex, expensive, and bulky. Another approach is to use passive components as shown in Fig. 1(b). This method balances LED currents automatically and it is largely divided into inductive method using coupled inductor or current sharing transformer and capacitive method using charge (amp–sec) balance condition on capacitor. In [4]–[7], LED balancing circuits using inductive method were introduced. They used coupled inductors to balance LED currents by current sharing mechanism of transformer action. In [8]–[17], on the other hand, various LED drivers using capacitive method were introduced. In [8], various LED drivers using capacitors to bridge-type circuits were introduced. In [9]–[12], multichannel LED drivers using resonant converter were employed to achieve the current balancing among LED strings. In [13]–[17], nonisolated LED drivers using capacitive current sharing mechanism and utilizing a coupled inductor were introduced. However, all the mentioned LED drivers require many semiconductor devices to balancing LED currents.

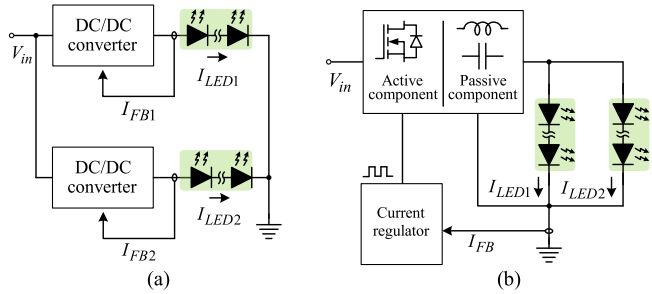

Fig. 1. Common methods for LED current balancing. (a) Separated converters. (b) Integrated converter with passive components.

Z-source inverter was first introduced in 2003 to overcome some technical barriers in the traditional voltage-fed (VF) and current-fed (CF) inverters [18]. Since then, it has been applied to multilevel converters [19], [20], dc–dc converters [21]–[23], and others [24]–[26]. Fig. 2 shows basic structures of the Z-source/quasi-Z-source (qZS) dc–dc converters. In the VF–Z-source shown in Fig. 2(a), the two capacitor voltages of the Z-source network are always balanced even if different value of loads are connected across the capacitors. In fact, the capacitor voltage balance is achieved by flux (volt–sec) balance condition on the two inductors in the Z-source network. The CF–Z-source shown in Fig. 2(b) is dual circuit of Fig. 2(a). Therefore, according to the duality principle, the two inductor currents in the Z-source network can be balanced even if different value of loads is connected in series with the inductors. The inductor current balance is achieved by charge (amp–sec) balance condition on the two capacitors in the Z-source network. Fig. 2(c) shows CF–qZS dc–dc converters [27]. When compared with Fig. 2(b), the CF–qZS provides common ground between input source and switching devices while the inductor current balancing is still maintained.

Manuscript received November 25, 2020; revised April 2, 2021; accepted May 19, 2021. Date of publication May 26, 2021; date of current version August 16, 2021. This work was supported by the National Research Foundation of Korea grant funded by the Korea government (NRF-2021R1A2C2007879). Recommended for publication by Associate Editor R.-L. Lin. *(Corresponding author: Honnyong Cha.)*

The authors are with the School of Energy Engineering, Kyungpook National University, Daegu 41566, South Korea (e-mail: hongda1021@knu.ac.kr; chahonny@knu.ac.kr).

Color versions of one or more figures in this article are available at https://doi.org/10.1109/TPEL.2021.3083842.

Digital Object Identifier 10.1109/TPEL.2021.3083842

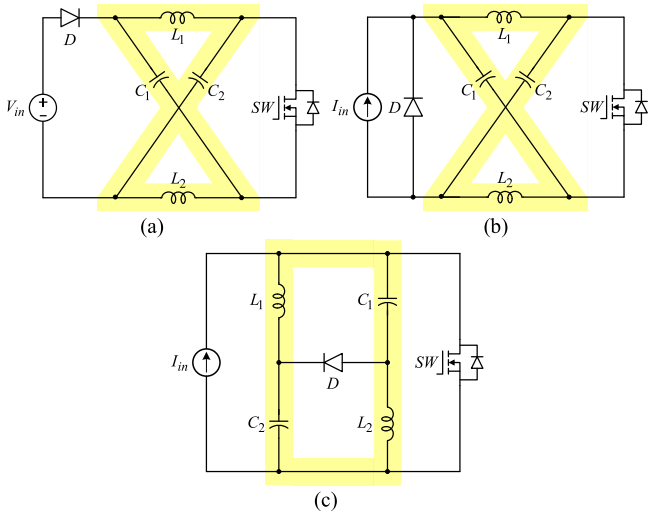

Fig. 2. Basic structure for Z-source dc–dc converters. (a) VF–Z-source. (b) CF–Z-source. (c) CF–quasi-Z-source.

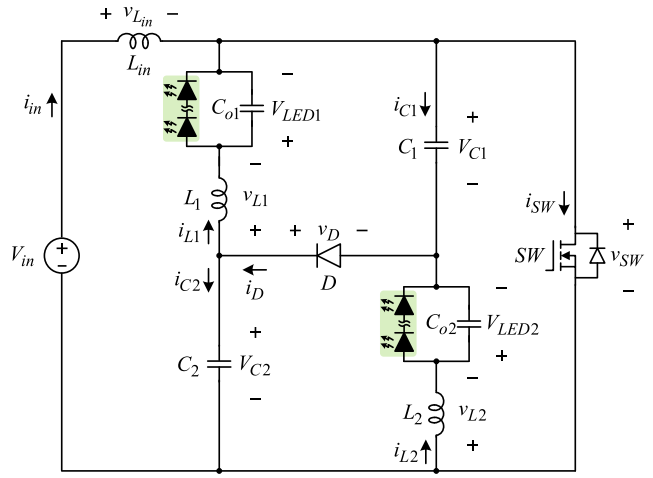

Fig. 3. Proposed two-channel LED driver using CF–qZS converter.

In this article, the CF–qZS network shown in Fig. 2(c) is applied to two-channel LED driver. Although many researches were conducted on the CF–qZS converter, the use of the CF–qZS converter on the current balancing has not been reported so far. To verify performance of the proposed converter, 80 W prototype is built and tested. Detailed operating principle of the proposed converter is explained in Section II. Section III presents some design considerations of the proposed LED driver. Experimental results and the conclusion of this article are discussed in Sections IV and V, respectively.

II. Operating Principle of the Proposed LED Driver

Fig. 3 shows the proposed two-channel LED driver. As already mentioned in the introduction, both CF–Z-source and CF–qZS converters can balance the two inductor currents. However, the CF–qZS is considered in this article because it has common ground feature, so low-side (nonisolated) gate driving circuit can be used. As shown in Fig. 3, the two LED strings and output

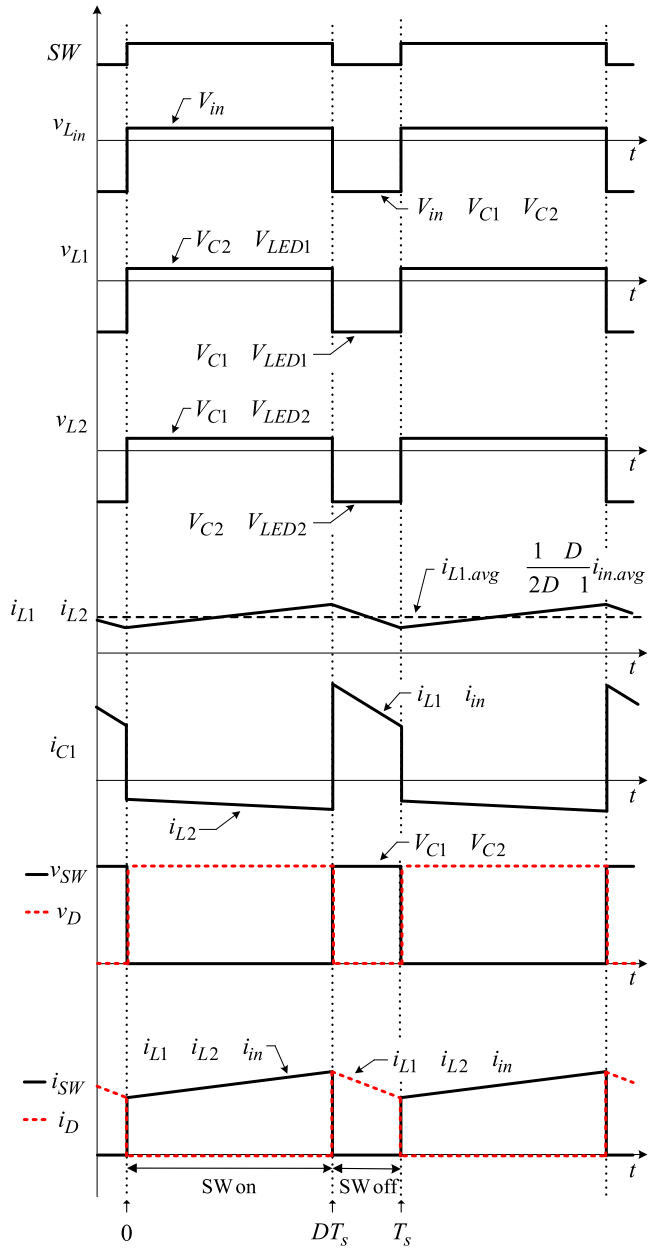

Fig. 4. Key waveforms of the proposed converter.

capacitors (C_{o1}, C_{o2})are connected in series with inductors L_1 and L_2, respectively. The output capacitors C_{o1} and C_{o2} are added to remove ripple component of inductor currents, thus both LED currents have only dc value. More importantly, if there are no output capacitors and LED is failure with open circuit, the inductor current drops to zero in a very short time because there is no current path, thus a huge voltage overshoot is generated.

A. Operation Mode Analysis

Key waveforms and operating modes of the proposed LED driver are shown in Figs. 4 and 5, respectively. As shown in Fig. 4, there are two operating modes. The switch is turned-ON and -OFF, respectively. For the sake of simplicity, it is assumed that all the semiconductor devices are ideal and the inductors

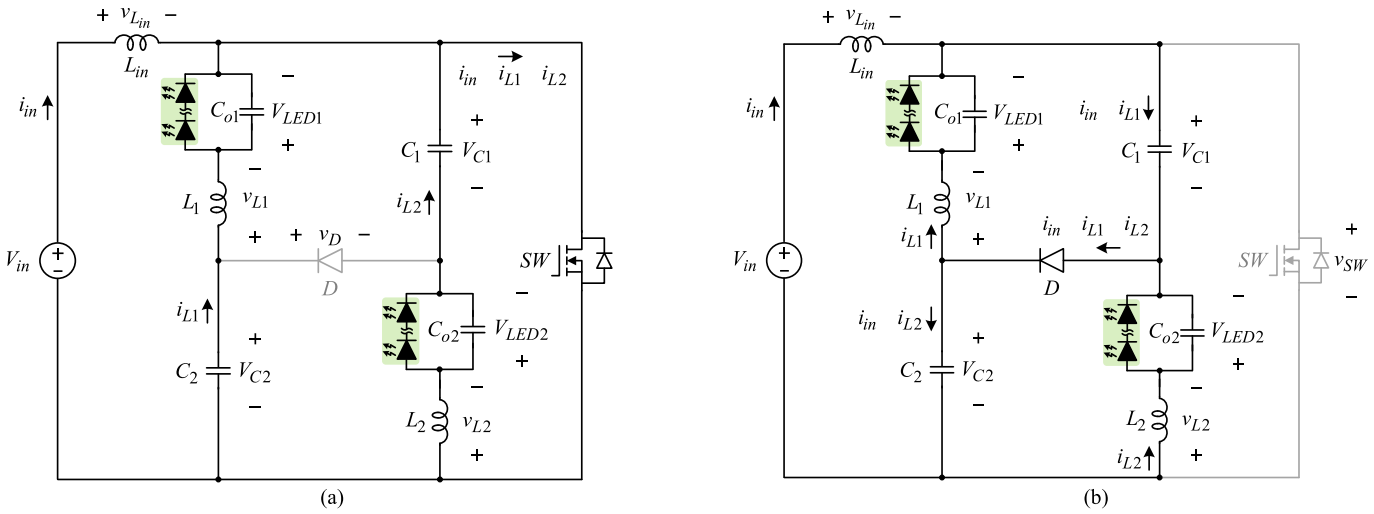

Fig. 5. Operation modes of the proposed converter. (a) Switch ON. (b) Switch OFF.

and capacitors in the qZS network have no equivalent series resistance. In addition, it is assumed that the capacitors C_1 and C_2 in the qZS network are big enough, thus the capacitor voltages V_{C1}, V_{C2} have only dc component with no ripple.

1) *Switch ON* ($0 < t \leq DT_s$): In this mode, the switch is turned-ON and diode is turned-OFF, as shown in Fig. 5(a). The input inductor $L_{\rm in}$ stores energy and the two capacitors C_1 and C_2 are discharged. The two inductor currents i_{L1} and i_{L2} are increasing and the two capacitor currents are as follows:

$$i_{C1} = -i_{L2}, \;\; i_{C2} = -i_{L1}. \tag{1}$$

Switch current $i_{\rm SW}$ is sum of the input current $i_{\rm in}$ and the two inductor currents (i_{L1}, i_{L2}). Diode voltage v_D is sum of the two capacitor voltages V_{C1} and V_{C2}.

2) *Switch OFF* ($DT_s < t \leq T_s$): In this mode, switch is turned-OFF and the diode is turned-ON to ensure inductor currents continue to flow, as shown in Fig. 5(b). Capacitors C_1 and C_2 are charged and the inductor currents are decreasing. i_{C1} is sum of the input current $i_{\rm in}$ and i_{L1}. Similarly, i_{C2} is sum of the input current $i_{\rm in}$ and i_{L2}. Thus, equations for the two capacitor currents in this mode are as follows:

$$i_{C1} = i_{\rm in} + i_{L1}, \;\; i_{C2} = i_{\rm in} + i_{L2}. \tag{2}$$

Similar to mode 1, diode current i_D is sum of the input current $i_{\rm in}$ and the two inductor currents (i_{L1}, i_{L2}). Also, the switch voltage $v_{\rm SW}$ is sum of the two capacitor voltages V_{C1} and V_{C2}.

B. LED Current Balancing and Voltage Gain

The proposed LED driver balances the two LED currents by charge balance condition on the capacitors C_1 and C_2. Fig. 4 shows the capacitor current i_{C1} waveform and i_{C2} can be found similarly. From (1) and (2), charge balance condition on the capacitors C_1 and C_2 are expressed as

$$C_1: \;\; D(-i_{L2.\rm avg}) + (1-D)(i_{in.\rm avg} + i_{L1.\rm avg}) = 0 \tag{3}$$

$$C_2: \;\; D(-i_{L1.\rm avg}) + (1-D)(i_{\rm in.avg} + i_{L2.\rm avg}) = 0 \tag{4}$$

where D is duty cycle of the switch. $i_{L1.\rm avg}$, $i_{L2.\rm avg}$, and $i_{\rm in.avg}$ represent average values of the inductor currents i_{L1}, i_{L2}, and input current $i_{\rm in}$, respectively. From (3) and (4), following expressions can be derived:

$$i_{L1.\rm avg} = i_{L2.\rm avg} \tag{5}$$

$$\frac{i_{L.\rm avg}}{i_{in.\rm avg}} = \frac{1-D}{2D-1}. \tag{6}$$

In (6), $i_{L.\rm avg}$ represents $i_{L1.\rm avg}$ and $i_{L2.\rm avg}$. From (5), it is found that the two LED string currents are precisely balanced regardless of external conditions such as different number of LEDs in string, unequal LED characteristics occurring in manufacturing process, and thermal conditions. Current gain of the proposed converter is shown in (6).

On the other hand, from the inductor voltage (v_{L1}, v_{L2}) waveforms in Fig. 4 and using flux balance condition on the inductors L_1 and L_2, following equations are derived:

$$L_1: \;\; D(V_{C2} - V_{\rm LED1}) = (1-D)(V_{C1} + V_{\rm LED1}) \tag{7}$$

$$L_2: \;\; D(V_{C1} - V_{\rm LED2}) = (1-D)(V_{C2} + V_{\rm LED2}). \tag{8}$$

From (7) and (8), capacitor voltages V_{C1} and V_{C2} are expressed as

$$V_{C1} = \frac{(1-D)V_{\rm LED1} + DV_{\rm LED2}}{2D-1} \tag{9}$$

$$V_{C2} = \frac{DV_{\rm LED1} + (1-D)V_{\rm LED2}}{2D-1}. \tag{10}$$

From (9) and (10), it is found that the two capacitor voltages V_{C1} and V_{C2} depend on LED string voltages ($V_{\rm LED1}$, $V_{\rm LED2}$)

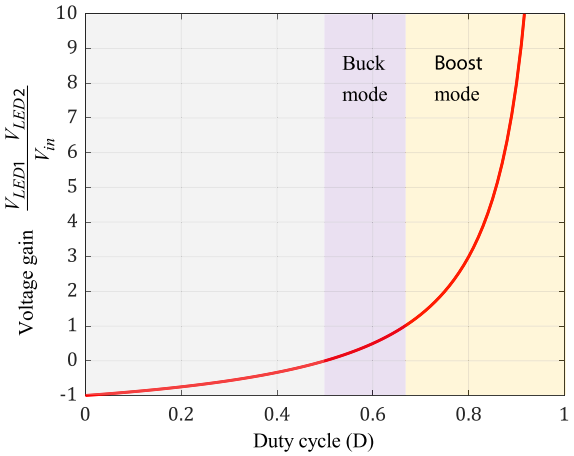

Fig. 6. Voltage gain of the proposed converter.

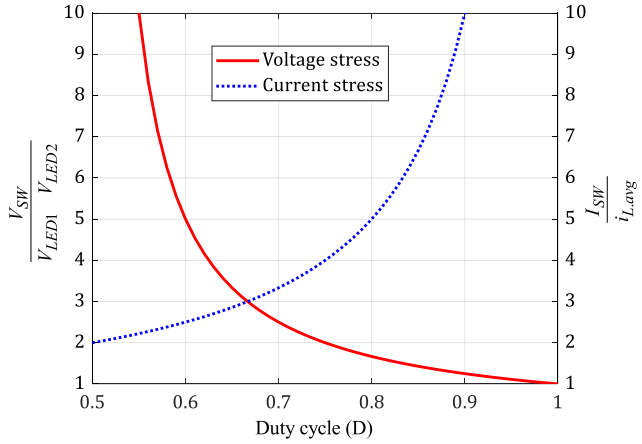

Fig. 7. Voltage and current stresses of switch.

and D. Thus, if voltages of LED1 and 2 are different, V_{C1} and V_{C2} are different. In addition, voltage of the input inductor $v_{L_{\rm in}}$ is shown as

$$v_{L_{\rm in}} = \begin{cases} V_{\rm in} & , \ (0 < t \le DT_s) \\ V_{\rm in} - V_{C1} - V_{C2} & , \ (DT_s < t \le T_s). \end{cases} \tag{11}$$

From (9)–(11) and using flux balance condition on the input inductor $L_{\rm in}$, voltage gain of the proposed converter can be obtained as

$$\frac{V_{\rm LED1} + V_{\rm LED2}}{V_{\rm in}} = \frac{2D-1}{1-D}. \tag{12}$$

Fig. 6 shows voltage gain of the proposed converter. The proposed converter has buck–boost function when the duty cycle is between 0.5 and 1. On the other hand, when $D < 0.5$, the voltage gain becomes negative. Thus, the proposed LED driver should be operated in the range of $0.5 < D < 1.0$ for proper steady-state operation. However, during start-up, D starts from zero, thus the LED strings experience negative voltage. Most of individual LEDs in a string can withstand at least 5 V in reverse direction [28]. Therefore, when selecting the number of LEDs in a string or input voltage $V_{\rm in}$, a care must be taken not to exceed the reverse voltage of LED. This issue will be discussed in Section III-D.

III. Design Considerations of the Proposed LED Driver and Comparisons With Other Topologies

In the proposed LED driver, several design issues exist as follows.

A. Voltage and Current Stresses of the Switch and Diode

In the proposed driver, the voltage stresses of switch and diode are sum of the two capacitor voltages. Thus, from (9)–(10), they can be derived as

$$V_{\rm SW} = V_D = \frac{V_{\rm LED1} + V_{\rm LED2}}{2D-1} \tag{13}$$

where $V_{\rm SW}$ and V_D are voltage of the switch and diode, when they are turned-OFF, respectively.

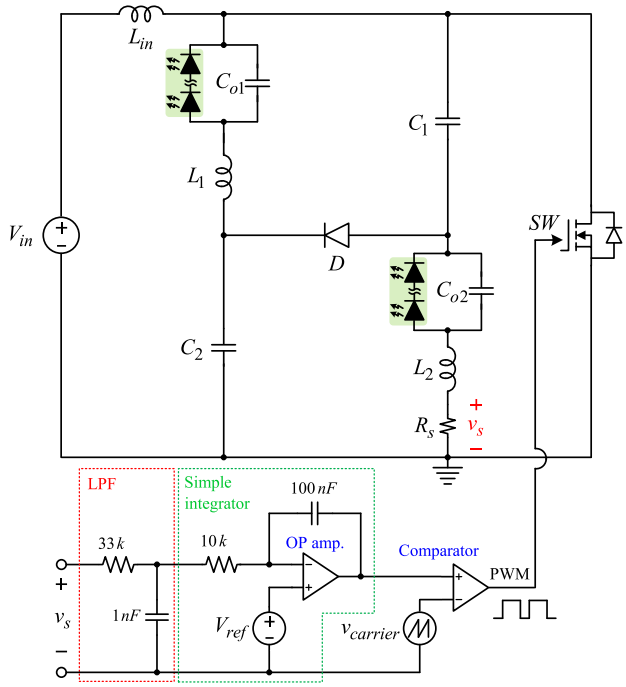

Fig. 8. Proposed converter with feedback circuit.

Similarly, switch and diode currents are sum of the input current ($i_{\rm in}$) and two inductor currents (i_{L1}, i_{L2}). Thus, by using (6), switch and diode currents are obtained as

$$I_{\rm SW} = I_D = \frac{i_{L.\rm avg}}{1-D} \tag{14}$$

where $I_{\rm SW}$ and I_D are currents flowing through the switch and diode, respectively, with ripple components are neglected. From (13) and (14), it is found that switch and diode voltages (or currents) depend on both LED voltages (or currents) and duty cycle (D).

Fig. 7 shows the voltage and current stresses of the switch. The LED voltages ($V_{\rm LED1}$, $V_{\rm LED2}$) and currents ($i_{L.\rm avg}$) can be assumed to be constant in steady state. Thus, switch voltage stress increases as D decreases. Therefore, switch voltage stress

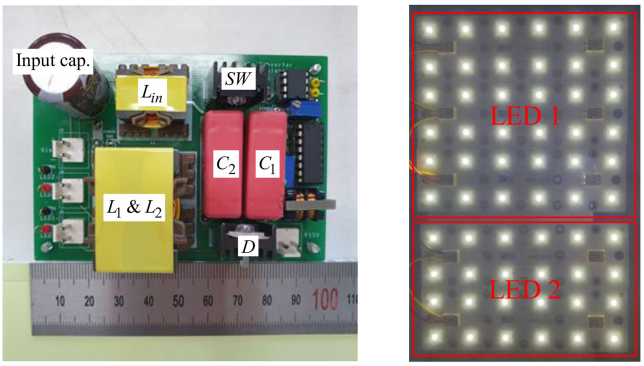

Fig. 9. (a) Photograph of prototype converter. (b) LED strings (HiLOM-RH12).

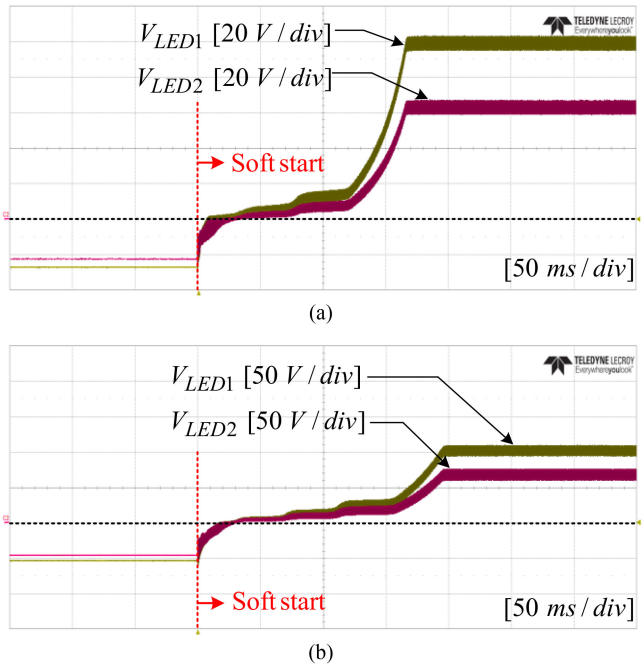

Fig. 10. LED voltages during soft-start. (a) $V_{\rm in} = 50$ V. (b) $V_{\rm in} = 100$ V.

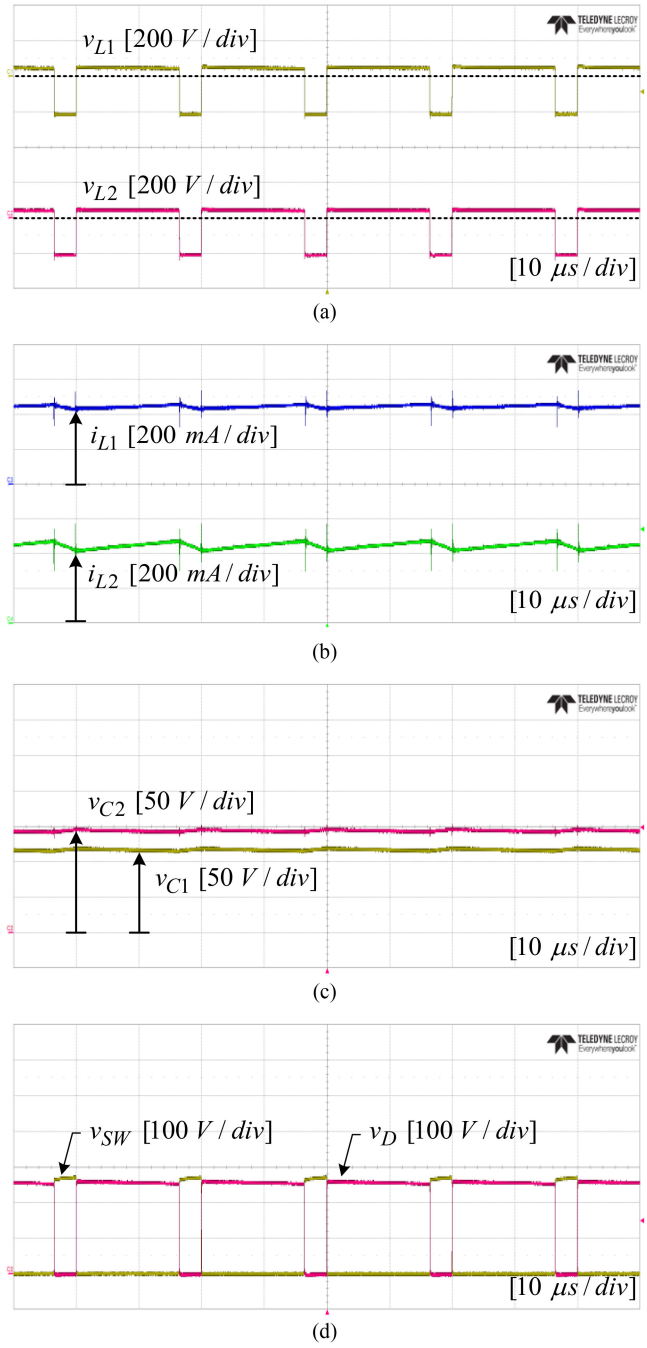

Fig. 11. Experimental waveforms when $V_{\rm in} = 50$ V, $i_{\rm ref} = 450$ mA. (a) qZS inductor voltages. (b) qZS inductor currents. (c) qZS capacitor voltages. (d) Switch and diode voltages.

is relatively high in buck mode (i.e., $0.5 < D < 2/3$). On the other hand, switch current stress increases as D increases. Therefore, it is relatively high in boost mode (i.e., $2/3 < D < 1$). In this article, the converter is designed to operate in boost mode to reduce switch voltage stress.

B. Inductor Current Ripple

From the inductor voltage waveforms in Fig. 4, inductor current ripples (Δi_{L1}, Δi_{L2}) are calculated as

$$\Delta i_{L1} = \frac{V_{C2} - V_{\rm LED1}}{L_1} DT_s \tag{15}$$

$$\Delta i_{L2} = \frac{V_{C1} - V_{\rm LED2}}{L_2} DT_s. \tag{16}$$

As shown in (15) and (16), the inductor current ripples are affected by capacitor voltages (V_{C1}, V_{C2}), LED voltages ($V_{\rm LED1}$, $V_{\rm LED2}$), inductances (L_1, L_2), period (T_s), and D. If inductance values or inductor voltages are different, two current ripples are unequal. However, as mentioned earlier, average values of the two inductor currents $i_{L1.\rm avg}$ and $i_{L2.\rm avg}$ are same by charge balance condition on the capacitors C_1 and C_2. As is well known, for the reduction of inductor current ripple,

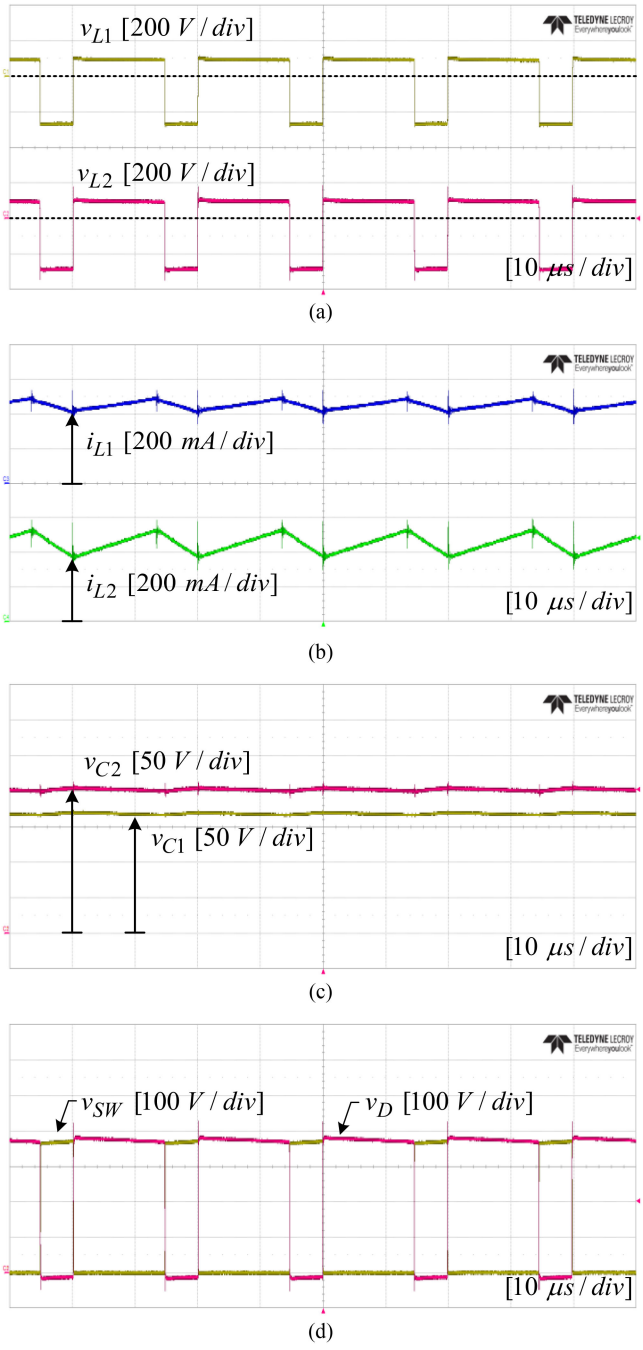

Fig. 12. Experimental waveforms when $V_{\rm in} = 100$ V, $i_{\rm ref} = 450$ mA. (a) qZS inductor voltages. (b) qZS inductor currents. (c) qZS capacitor voltages. (d) Switch and diode voltages.

high inductance is preferred. However, the size of inductor is increased. Therefore, a trade-off should be made.

C. Gate Driving and Feedback Circuit

Fig. 8 shows the proposed LED driver with feedback circuit. As shown, in the proposed converter, source terminal of the MOSFET is common to the input voltage $V_{\rm in}$, thus low-side gate driving circuit can be used. In addition, since average values of the two LED currents are well balanced, only one LED current

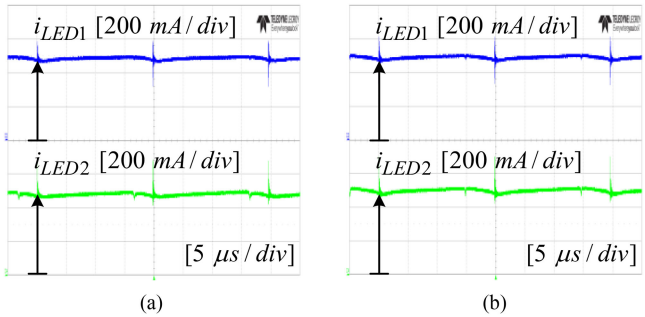

Fig. 13. LED currents waveform: (a) when $V_{\rm in} = 50$ V and (b) when $V_{\rm in} = 100$ V.

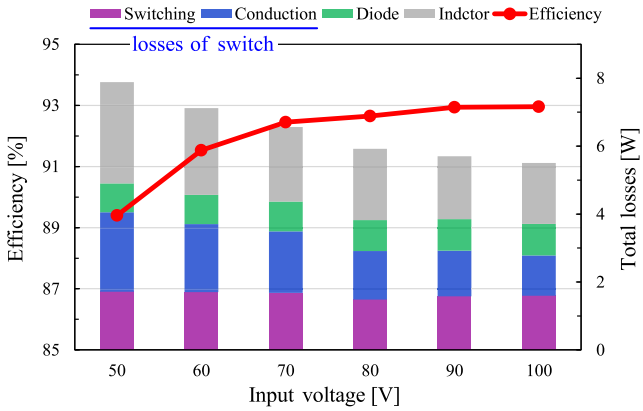

Fig. 14. Measured efficiency and loss analysis of the proposed LED driver.

needs to be sensed for current control. In this article, inductor current i_{L2} is sensed by connecting sensing resistor R_s in series with L_2. To filter out high-frequency current ripple and sense average value of the inductor current, an RC low-pass filter (LPF) is added to feedback compensation and the output of the LPF is compared with $V_{\rm ref}$ which is reference voltage across the sensing resistor. In this article, an RC LPF with 4.8 kHz cut-off frequency ($R_{\rm LPF} = 33\,{\rm k}\Omega, C_{\rm LPF} = 1\,{\rm n}F$) is added and simple integrator having 1 ms time constant ($R_F = 10\,{\rm k}\Omega$, $C_F = 100$ nF) is applied to control LED currents.

D. LED Voltage and Input Voltage Range

As discussed in Section II-B, reverse voltage is applied to the two LED strings during soft-start or start-up. Before the start ($D = 0$), sum of the two LED voltages is equal to $-V_{\rm in}$ (i.e., $V_{\rm LED1} + V_{\rm LED2} = -V_{\rm in}$). Thus, when designing a hardware, input voltage range, and number of LEDs must be decided carefully. If we define n_1 and n_2 as the number of LEDs in strings 1 and 2, respectively, and V_r as reverse blocking voltage of each LED, then the maximum input voltage should be smaller than $(n_1 + n_2)V_r$.

E. Comparisons With Other LED Drivers

The proposed LED driver was compared with various noniso-lated drivers using capacitive method to balance LED currents.

TABLE I
COMPARISONS WITH OTHER LED DRIVERS USING CAPACITIVE METHOD

	No. of channel	No. of switch	No. of diode	No. capacitor	No. of magnetics	Gate driving	Switch voltage
Driver in [13]	2	2	2	4	2	High-side	V_{in}
Driver in [14]	2	2	2	3	2	High-side	$\frac{V_{LED1}}{V_{LED1}+V_{LED2}}V_{in}, V_{in}$
Driver in [16]	2	1	3	3	1	Low-side	$D(V_{LED1}+V_{LED2})$
Proposed driver	2	1	1	4	2 (L_1&L_2 are coupled)	Low-side	$\frac{V_{LED1}+V_{LED2}}{2D-1}$

TABLE II
ELECTRICAL SPECIFICATIONS OF THE PROPOSED CONVERTER

Parameter	Value
Input voltage (V_{in})	50 – 100 V
LED current ($i_{L1,avg}$, $i_{L2,avg}$)	450 mA / channel
Number of LED	36, 24
Switching frequency	50 kHz
Input inductance (L_{in})	2 mH
qZS inductance (L_1, L_2)	11 mH
qZS capacitance (C_1, C_2)	2.2 μF
Output capacitance (C_{o1}, C_{o2})	100 nF
MOSFET	SPP20N60CFD
Diode	C3D0806A

Table I shows a brief comparison with other LED drivers. Drivers in [13] and [14] use two switches. Although their voltage stresses are always equal to or less than input voltage, they require high-side (isolated) gate driving which implies more complicated gate driving circuity. Driver in [16] uses one switch and low-side gate driving is used owing to common ground feature.

The proposed LED driver also uses low-side gate driver, but switch voltage depends on duty cycle and it is always greater than input voltage. However, the proposed LED driver uses only one active switch and one diode to balance two-channel currents and its operation mode is simple.

IV. EXPERIMENTAL RESULTS

In order to verify performance of the proposed converter, 80 W prototype converter was built and tested. Fig. 9(a) shows the prototype converter and the two LED strings used in the experiment are shown in Fig. 9(b). Each LED used in the experiment can endure more than -10 V reverse voltage and flow 1500 mA forward current. The two inductors L_1 and L_2 are coupled together using PQ32/30 ferrite core. Large input inductance value is required to implement a current source. Too large input inductance, however, increases total volume of the converter. Therefore, input inductor design requires trade-off similar to the qZS inductor (L_1, L_2) design. In this article, the input inductor $L_{\rm in}$ is designed using PQ20/16 ferrite core. UC3823 PWM IC is used for feedback control and gate signal generation. Table II shows electrical specifications of the prototype converter used in experiment. In order to verify the current balancing under severe mismatched condition, different number of LEDs is connected in each string (i.e., 36 for LED 1 and 24 for LED 2).

Fig. 10 shows the LED voltage waveforms during soft-start (start-up). As mentioned in Section III-D, before the start-up, sum of the two LED voltages are equal to $-V_{\rm in}$. As the gate signal is applied and D is gradually increased from zero, the LED voltages increase from negative to positive values causing LEDs turn-ON. Figs. 11 and 12 show experimental waveforms of the proposed converter tested under the conditions in Table II. Fig. 11 shows waveforms with $V_{\rm in} = 50$ V and $D = 0.81$. Fig. 12 shows waveforms with $V_{\rm in} = 100$ V and $D = 0.72$. In addition, LED currents are shown in Fig. 13 when $V_{\rm in} = 50$ V and $V_{\rm in} = 100$ V, respectively. As shown, the average values of the LED currents are well balanced even if different number of LEDs is connected. It can also be seen that the capacitor voltages (V_{C1}, V_{C2}) are not equal and the difference is caused by the different LED voltages. In addition, as input voltage increases (duty cycle is decreased), the capacitor voltages also increase. As a result of this, switch and diode voltage stresses also increase. Fig. 14 shows measured efficiency and loss analysis of the proposed LED driver as $V_{\rm in}$ varies with same output power. As the input voltage increases, the efficiency also increases because conduction losses of inductors and semiconductor devices are decreased.

V. CONCLUSION

In this article, two-channel LED driver using the CF–qZS converter was proposed. Owing to the unique current balancing feature of the CF–qZS network, LED currents are precisely balanced. The proposed circuit requires only one switch and one diode. In addition, input current is continuous and low-side gate driving is possible. The proposed LED driver was verified through experiments.

REFERENCES

[1] N. Narendran and Y. Gu, "Life of LED-based white light sources," *J. Display Technol.*, vol. 1, no. 1, pp. 167–171, Sep. 2005.
[2] P. Liu, Y. Hsu, and S. Hsu, "Drain-voltage balance and phase-shifted PWM control schemes for high-efficiency parallel-string dimmable LED drivers," *IEEE Trans. Ind. Electron.*, vol. 65, no. 8, pp. 6168–6176, Aug. 2018.
[3] G. Carraro, "Solving high-voltage off-line HB-LED constant current control-circuit issues," in *Proc. 22nd Annu. IEEE Appl. Power Electron. Conf. Expo.*, 2007, pp. 1316–1318.

[4] X. Wu, Z. Wang, and J. Zhang, "Design considerations for dual-output quasi-resonant flyback LED driver with current-sharing transformer," *IEEE Trans. Power Electron.*, vol. 28, no. 10, pp. 4820–4830, Oct. 2013.
[5] K. I. Hwu, W. C. Tu, and M. J. Hong, "A dimmable LED driver based on current balancing transformer with magnetizing energy recycling considered," *J. Display Technol.*, vol. 10, no. 5, pp. 388–395, May 2014.
[6] Y. Lin, H. Chiu, Y. Lo, and C. Leng, "LED backlight driver circuit with dual-mode dimming control and current-balancing design," *IEEE Trans. Ind. Electron.*, vol. 61, no. 9, pp. 4632–4639, Sep. 2014.
[7] Y. Lin, H. Chiu, Y. Lo, and C. Leng, "Light-emitting diode driver with a combined energy transfer inductor for current balancing control," *IET Power Electron.*, vol. 8, no. 10, pp. 1834–1843, Sep. 2015.
[8] J. Wang, J. Zhang, X. Huang, and L. Xu, "A family of capacitive current balancing methods for multi-output LED drivers," in *Proc. 26th Annu. IEEE Appl. Power Electron. Conf. Expo.*, 2011, pp. 2040–2046.
[9] X. Wu, J. Zhang, and Z. Qian, "A simple two-channel LED driver with automatic precise current sharing," *IEEE Trans. Ind. Electron.*, vol. 58, no. 10, pp. 4783–4788, Oct. 2011.
[10] S. Choi and T. Kim, "Symmetric current balancing circuit for LED backlight with dimming," *IEEE Trans. Ind. Electron.*, vol. 59, no. 4, pp. 1698–1707, Apr. 2012.
[11] X. Chen, D. Huang, Q. Li, and F. C. Lee, "Multichannel LED driver with CLL resonant converter," *IEEE J. Emerg. Sel. Topics Power Electron.*, vol. 3, no. 3, pp. 589–598, Sep. 2015.
[12] X. Liu, Q. Yang, Q. Zhou, J. Xu, and G. Zhou, "Single-stage single-switch four-output resonant LED driver with high power factor and passive current balancing," *IEEE Trans. Power Electron.*, vol. 32, no. 6, pp. 4566–4576, Jun. 2017.
[13] K. I. Hwu and W. Z. Jiang, "Nonisolated two-channel LED driver with automatic current balance and zero-voltage switching," *IEEE Trans. Power Electron.*, vol. 31, no. 12, pp. 8359–8370, Dec. 2016.
[14] D. Do, H. Cha, B. L. Nguyen, and H. Kim, "Two-channel interleaved buck LED driver using current-balancing capacitor," *IEEE J. Emerg. Sel. Topics Power Electron.*, vol. 6, no. 3, pp. 1306–1313, Sep. 2018.
[15] K. I. Hwu and W. Z. Jiang, "Nonisolated two-phase interleaved LED driver with capacitive current sharing," *IEEE Trans. Power Electron.*, vol. 33, no. 3, pp. 2295–2306, Mar. 2018.
[16] J. Kim, J. Choe, and J. J. Lai, "Nonisolated single-switch two-channel LED driver with simple lossless snubber and low-voltage stress," *IEEE Trans. Power Electron.*, vol. 33, no. 5, pp. 4306–4316, May 2018.
[17] X. Liu, Y. Wan, Z. Dong, M. He, Q. Zhou, and C. K. Tse, "Buck–boost–buck-type single-switch multistring resonant LED driver with high power factor and passive current balancing," *IEEE Trans. Power Electron.*, vol. 35, no. 5, pp. 5132–5143, May 2020.
[18] F. Z. Peng, "Z-source inverter," *IEEE Trans. Ind. Appl.*, vol. 39, no. 2, pp. 504–510, Mar./Apr. 2003.
[19] P. C. Loh, S. W. Lim, F. Gao, and F. Blaabjerg, "Three-level Z-source inverters using a single LC impedance network," *IEEE Trans. Power Electron.*, vol. 22, no. 2, pp. 706–711, Mar. 2007.
[20] B. Ge, Y. Liu, H. Abu-Rub, and F. Z. Peng, "State-of-charge balancing control for a battery-energy-stored quasi-Z-source cascaded-multilevel-inverter-based photovoltaic power system," *IEEE Trans. Ind. Electron.*, vol. 65, no. 3, pp. 2268–2279, Mar. 2018.
[21] D. Cao and F. Z. Peng, "A family of Z-source and quasi-Z-source dc-dc converters," in *Proc. 24th Annu. IEEE Appl. Power Electron. Conf. Expo.*, 2009, pp. 1097–1101.
[22] H. Shen, B. Zhang, D. Qiu, and L. Zhou, "A common grounded Z-source dc–dc converter with high voltage gain," *IEEE Trans. Ind. Electron.*, vol. 63, no. 5, pp. 2925–2935, May 2016.
[23] A. Torkan and M. Ehsani, "A novel nonisolated Z-source dc–dc converter for photovoltaic applications," *IEEE Trans. Ind. Appl.*, vol. 54, no. 5, pp. 4574–4583, Sep./Oct. 2018.
[24] O. Ellabban, H. Abu-Rub, and S. Bayhan, "Z-source matrix converter: An overview," *IEEE Trans. Power Electron.*, vol. 31, no. 11, pp. 7436–7450, Nov. 2016.
[25] H. Zeng, X. Wang, and F. Z. Peng, "High power density Z-source resonant wireless charger with line frequency sinusoidal charging," *IEEE Trans. Power Electron.*, vol. 33, no. 12, pp. 10148–10156, Dec. 2018.
[26] J. Shu, S. Wang, J. Ma, T. Liu, and Z. He, "An active Z-source dc circuit breaker combined with SCR and IGBT," *IEEE Trans. Power Electron.*, vol. 35, no. 10, pp. 10003–10007, Oct. 2020.
[27] J. Anderson and F. Z. Peng, "Four quasi-Z-source inverters," in *Proc. IEEE Power Electron. Specialists Conf.*, 2008, pp. 2743–2749.
[28] R. Lenk and C. Lenk, "Practical characteristics of LEDs" in *Practical Lighting Design With LEDs*, 2nd ed., R. Lenk and C. Lenk, Eds. Hoboken, NJ, USA: Wiley, 2017, pp. 43–56.

Daheon Hong received the B.S. degree in 2020 from the School of Energy Engineering, Kyungpook National University, Daegu, South Korea, where he is currently working toward the M.S. degree.

His research interests include dc–dc converters, automatic current balancing, and high-frequency magnetics design.

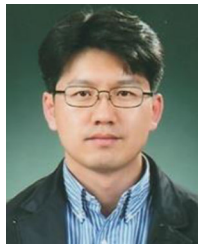

Honnyong Cha (Senior Member, IEEE) received the B.S. and M.S. degrees in electronics engineering from Kyungpook National University, Daegu, South Korea, in 1999 and 2001, respectively, and the Ph.D. degree in electrical engineering from Michigan State University, East Lansing, MI, USA, in 2009.

From 2001 to 2003, he was a Research Engineer with the Power System Technology Company, Ansan, South Korea. From 2010 to 2011, he was a Senior Researcher with the Korea Electrotechnology Research Institute, Changwon, South Korea. In 2011, he joined the School of Energy Engineering, Kyungpook National University. In 2017, he was a Visiting Scholar with the Future Energy Electronics Center, Virginia Polytechnic Institute and State University, Blacksburg, VA, USA. His research interests include high-power dc–dc converters, dc–ac inverters, Z-source inverters, and power conversion for electric vehicles and wind power generation.